Chinese Journal of
POLYMER SCIENCE

RESEARCH ARTICLE

https://doi.org/10.1007/s10118-024-3180-y
Chinese J. Polym. Sci. **2024**, *42*, 1768–1779

Robust Composite Separator Randomly Interwoven by PI and Pre-oxidized PAN Nanofibers for High Performance Lithium-ion Batteries

Ying Li[a], Chen Pan[a], Feng Gan[b*], Zhi-Xun Lin[a], Jin-Chao Yu[a], Zhen-Zhen Wei[a*], and Yan Zhao[a]

[a] *College of Textile and Clothing Engineering, National Engineering Laboratory for Modern Silk, Soochow University, Suzhou 215123, China*
[b] *College of Textile Science and Engineering, Wuyi University, Jiangmen 529020, China*

Abstract Electrospun nanofibrous separators, despite lacking superior mechanical strength, have gained widespread attention with high porosity and facile processing. Herein, utilizing the fact that thermal imidization temperature of poly(amic acid) (PAA) into polyimide (PI) coincides with the pre-oxidation temperature of polyacrylonitrile (PAN) into carbon fiber, we proposed a new cross-electrospinning strategy to obtain a composite nanofibrous separator (PI/oPAN) randomly interwoven by PI and pre-oxidized PAN (oPAN) nanofibers, *via* synchronously electrospinning the PAA and PAN onto the same collector and then heat-treating for 2 h at 300 °C. The resultant PI/oPAN separator was able to preserve high porosity (71.7%), electrolyte wettability and thermal stability of PI nanofibrous membrane, and surprisingly exhibited high mechanical strength, being 3 times of PI, which mainly because of the numerous adhesion points generated by the melting of PAN in the pre-oxidation process. Meanwhile, the polar groups of oPAN and 3D fibrous network enhanced the PI/oPAN separator's ionic conductivity and Li^+ transference number, rendering the corresponding cell with more stable cycling performance than cells assembled with pure PI, PAN or commercial PP separator. Therefore, this work might provide a new avenue for the ongoing design and further development of LIB separators capable of high safety and high performance.

Keywords Lithium-ion battery; Nanofibrous separator; Cross-electrospinning; Polyimide; Pre-oxidized polyacrylonitrile

Citation: Li, Y.; Pan, C.; Gan, F.; Lin, Z. X.; Yu, J. C.; Wei, Z. Z.; Zhao, Y. Robust composite separator randomly interwoven by PI and pre-oxidized PAN nanofibers for high performance lithium-ion batteries. *Chinese J. Polym. Sci.* **2024**, *42*, 1768–1779.

INTRODUCTION

Lithium-ion batteries (LIBs), a kind of essential energy storage equipment, have been applied in the field of electric vehicles and mobile devices on account of their strong points of high energy density, high power, excellent cycle performance, no memory effect, and low environmental pollution.[1–3] LIBs contain a cathode, anode, electrolyte and separator. Among them, the separator is a kind of thin membrane featuring a microporous structure that isolates the cathode and anode in the battery and simultaneously acts as a channel for the transport of Li^+, thus having a major contribution to the performance and safety of LIBs.[4,5]

Currently, most commercial LIBs use microporous polyolefin separators, whose main materials are polypropylene (PP) and polyethylene (PE), with low separator thickness and the merits of strong mechanical strength, high chemical and electrochemical stability as well as low cost.[6] However, when a large amount of heat is generated by the battery during the thermal runaway process, the battery's internal temperature will keep rising and the polyolefin separator will begin to shrink and melt, leading to short circuits or even explosions inside the battery.[7] On the other hand, the microporous polyolefin separators face problems like low porosity (40%–60%)[8] and poor wettability, which may contribute to the formation of lithium dendrites inside the battery,[9] which not only cause irreversible loss of active material at the anode and drastically diminish the battery's capacity, but also penetrate the separator, triggering a short circuit and creating a potential safety hazard. For the further development of LIBs, research and development of new separators is therefore of great importance.

Compared with the traditional nonwoven mats, the electrospun nanofibrous membrane has a finer diameter and smaller pore size, which is beneficial to alleviate the self-discharge phenomenon of the battery.[10] Meanwhile, the nanofibrous membrane with high porosity (70%–90%) and three-dimensional (3D) network structure also forms a good channel for the migration of Li^+.[11,12] Currently, many polymer materials such as polyimide (PI),[13,14] polyacrylonitrile (PAN),[15,16] poly(vinylidene fluoride) (PVDF),[17,18] poly(vinyl alcohol) (PVA),[19] poly(ethylene terephthalate) (PET),[20] *etc.*, have already been prepared by electrospinning for LIB separators. Representatively, electrospun PI or PAN nanofibrous separators have drawn increasing concern because of their better thermal dimensional stability, mechanical properties and electrolyte wettability than polyolefin separators,[21–23] as

* Corresponding authors, E-mail: gf@dhu.edu.cn (F.G.)
E-mail: zzwei@suda.edu.cn (Z.Z.W.)

Received April 12, 2024; Accepted June 3, 2024; Published online September 13, 2024

well as those PI/PAN composite separators prepared by the hybrid solution of PAN and PI[24] or PAN blended with the monomers of PI.[25,26]

PI nanofibrous membrane is usually prepared by first electrospinning its precursor poly(amic acid) (PAA) solution, subsequently turning the PAA nanofibrous membrane into PI nanofibrous membrane by thermal imidization at around 300 °C.[13,27] Meanwhile, PAN undergoes pre-oxidation during the formation of carbon fibers, and the pre-oxidation refers to obtaining the pre-oxidized PAN (oPAN) at a temperature of 200–300 °C,[28] during which cyclization, dehydrogenation, cracking and oxidation reactions occur,[29] thus converting the linear PAN macromolecules into a more stable ladder structure which provides high thermal stability to the oPAN.[30] Since the pre-oxidation temperature of PAN is consistent with the thermal imidization of PAA, PI has already been combined with oPAN. Cao *et al*.[31] fabricated a sandwich composite separator *via* press-laminating two layers of PAA membranes formed by non-solvent phase separation on one layer of electrospun PAN nanofibrous membrane, and then stepwise heating to 250 °C for producing the PI and oPAN composite separator. Compared with pure PAN and PI separators, the resulting composite separator has the highest tensile strength, high thermal safety stability and excellent cycling performance retaining up to 94.3% of its capacity after 100 cycles at 1 C.

However, the PI/PAN composite membranes obtained by the above-mentioned methods have some inevitable problems. For the hybrid solution electrospinning method, (1) because the electrospinning solution concentration is limited by the mixing of the two components, it's difficult to achieve the optimum concentration to get the best fibrous property of each component; (2) it is impossible to select a uniform and suitable spinning condition including voltage and collection distance for both components; (3) there are compatibility problems with the components resulting in more weak joints, which, in turn, will affect the membrane's general mechanical properties. For the phase separation and lamination method, unstable surface bonding and falling off during use possibly occur besides the relatively complex fabrication process. Therefore, if the two spinning solutions are spun separately but collected to form a membrane, the respective performance advantages of the two components may be fully utilized, but few relevant studies have been reported so far.

Therefore, different from the hybrid solution electrospinning and lamination methods, in this work, we proposed a novel method called cross-electrospinning combined with heat treatment process to fabricate the PI/oPAN nanofibrous composite separator. As shown in Fig. 1, cross-electrospinning means that the PAA spinning solution and PAN spinning solution are controlled respectively by two sets of propulsion pumps and then spun onto the same target rotating collector where fibers are crossed and stacked to form a membrane. The obtained PI/oPAN separator had high porosity due to the porous network structure generated by the randomly interwoven nanofibers, the PI component ensured its thermal dimensional stability, and the adhesion points generated during the pre-oxidation step of PAN improved the mechanical properties of the composite separator, while the assembled Li/$LiFePO_4$ coin cells exhibited better cycling performance and rate capability compared to the one with PP separator.

EXPERIMENTAL

Materials

4,4′-Diaminophenyl ether (ODA), pyromellitic dianhydride (PMDA), polyacrylonitrile (PAN), *N*,*N*′-dimethylacetamide (DMAc), *n*-butanol, poly(vinylidene fluoride) (PVDF) and *N*-methyl-2-pyrrolidone (NMP) were purchased from Aladdin Chemical Reagents Co., Ltd., China. Lithium iron phosphate ($LiFePO_4$), lithium metal (Li), acetylene black (AB), and lithium hexafluorophosphate ($LiPF_6$, 1 mol/L) in ethylene carbonate, ethylmethyl carbonate, and dimethyl carbonate (EC:EMC:DMC=1:1:1 by volume) were purchased from Ferro Corp. The commercial PP separator (Celgard 2400) of approximately 25 μm in thickness was chosen as the comparator. All chemicals were used as they were received and not further purified or reconstituted.

Preparation of Cross-electrospun PI/oPAN Composite Nanofibrous Separator

As illustrated in Fig. 1, the cross-electrospun PI/oPAN composite

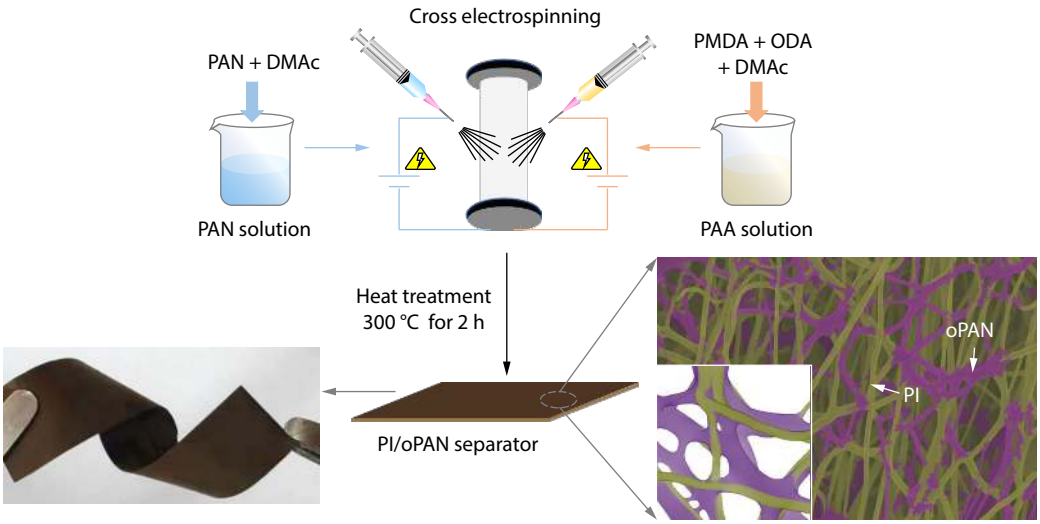

Fig. 1 Schematic illustration of manufacturing process of the PI/oPAN composite separator *via* cross-electrospinning and heat treatment.

https://doi.org/10.1007/s10118-024-3180-y

nanofibrous separator can be fabricated *via* the following two steps. Firstly, the PAA/PAN nanofibrous membrane was cross-electrospun. Some amount of ODA was dissolved in the DMAc by agitation for about 1 h, and then drop added a certain amount of PMDA powder with stirring for 12 h until this reaction was finished to obtain a 25 wt% PAA spinning solution. A 10 wt% PAN spinning solution was obtained by dissolution of a quantity amount of PAN powder in DMAc with constant agitation for 24 h. The spinning voltage and receiving interval for each solution were set as follows: (1) PAA: 18 kV and 18 cm; (2) PAN: 15 kV and 15 cm. The pushed rates of both solutions were the same and fixed at 1 mL/h. After spinning for 2 h, the electrospun membrane was kept in an oven to remove residual solvent for 4 h at 60 °C. Secondly, the obtained PAN/PAA nanofibrous composite membrane was heated at 300 °C for 2 h. This heat treatment can make the imidization of PAA and per-oxidation of PAN, so the PI/oPAN composite separator was obtained. For the sake of comparison, electrospun pure PI and PAN nanofibrous membranes were made under the above conditions, and the PAN membrane was without heat treatment.

Characterizations

The morphologies of the upper surface of the nanofibrous membranes were investigated with a field-emission scanning electron microscope (FE-SEM, S4800, Hitachi). The chemical structure changes during the imidization of PAA and per-oxidation of PAN process of the membranes were reflected in the range of 450–4000 cm^{-1} from Fourier transform infrared spectroscopy (FTIR, Nicolet 5700). The porosity of the nanofibrous membranes was measured by soaking the dry membrane in *n*-butanol for 2 h. The excess *n*-butanol on the membrane's surface was slightly absorbed with weighing paper and each kind of membrane was tested for five times. The porosity was then calculated using the equation:

$$\text{Porosity}\ (\%) = \frac{W_2 - W_1}{\rho V} \times 100\% \tag{1}$$

where ρ stands for *n*-butanol's density, V represents the round membrane's volume based on its diameter and thickness, and W_1 and W_2 are respectively the membrane's masses before and after being soaked in the *n*-butanol.

The contact angle of the nanofibrous membranes was monitored using an optical contact angle testing instrument (Dataphysics OCA100, Germany) and the full spreading times after a drop of electrolyte placed on the membrane were also recorded. The electrolyte uptake (EU) was figured out by dipping each kind of membrane for five times 2 h in the liquid electrolyte following the equation:

$$\text{EU}\ (\%) = \frac{W - W_0}{W_0} \times 100\% \tag{2}$$

where W_0 and W stand for masses of the membrane before and after infiltrated into electrolyte, respectively.

An Instron 3369 Universal Strength Tester was used to determine the mechanical properties. The tensile strength was performed at a stretching speed of 20 $mm{\cdot}min^{-1}$ with a clamping length of 20 mm and a gauge breadth of 10 mm. The puncture resistance was undertaken by piercing the membrane at a steady rate of 50 $mm{\cdot}min^{-1}$ with a 2.5 mm diameter needle. For both tensile and puncture tests, the data was averaged from five specimens per sample.

For thermal stability analysis, a thermogravimetric analyzer (TG, SDT-Q600) was utilized to subject the sample to heating under nitrogen at a rate of 10 $°C{\cdot}min^{-1}$ from 30 °C to 600 °C. Meantime, after heat treatment at room temperature, 100, 150 and 200 °C for 30 min, the membrane's dimensional stability was investigated by observing its heat shrinkage.

Electrochemical Measurements

An electrochemical workstation (BioLogic SP-300) was used to test the electrochemical properties of separators. To evaluate the separator's electrochemical stability window through the linear sweep voltammetry (LSV), coin cells were assembled by putting the separator infiltrated with liquid electrolyte between the stainless steel and Li. The LSV tests were all taken between 2.5 and 5.2 V versus Li/Li^+ at a scan rate of 10 mV/s. The bulk impedance of different separators was investigated through the electrochemical impedance spectroscopy (EIS) with an amplitude of 5 mV and a frequency range of 0.1 Hz–0.1 MHz by assembling corresponding cells, *via* putting the separator infiltrated with liquid electrolyte between two stainless steels. The ionic conductivity (σ) of different separators was then calculated *via* the equation:

$$\sigma = \frac{d}{R_b \times S} \tag{3}$$

where R_b is the bulk resistance deprived of the Nyquist plot, S stands for the cross-sectional area, and d represents the separator's thickness.

The lithium-ion transference number (t_{Li^+}) was figured out *via* alternating current (AC) impedance and direct current (DC) polarization techniques with coin cells assembled by placing the separator soaked with liquid electrolyte between two Li metal sheets using the question:

$$t_{Li^+} = \frac{I_s\,(V - I_0R_0)}{I_0\,(V - I_sR_s)} \tag{4}$$

where I_0 and I_s respectively stand for the initial and steady-state current values, R_0 and R_s denote to the cell's resistance before and after polarization, and V represents the applied voltage.

CR 2025 coin cells with PI, PAN, PI/oPAN and PP separators were used for measuring cycling performance and rate capability with a charge/discharge cycle tester (BTS 5 V 10 mA, Neware Company, China). The separator immersed with liquid electrolyte was laid between the $LiFePO_4$ cathode and Li anode. The $LiFePO_4$ cathode was made in advance, in which PVDF (polymer binder), AB (conductive additive), and $LiFePO_4$ (active material) were added in sequence with a mass ratio of 8:1:1 into NMP. After sufficient mixing, the pole piece obtained by knife coating was put into the vacuum for drying at 110 °C for 8 h. Firstly, the cell was activated at 0.2 C for 5 cycles with a potential range from 2.5 V to 4.2 V. After that, the cell's cycling performance was characterized at 1 C for 100 cycles. Rate capability measurements were performed by charging and discharging at diverse current densities of 0.2, 0.5, 1, 2 and 5 C.

RESULTS AND DISCUSSION

Morphological Analysis

The photographs of single-component and bicomponent nanofibrous membranes prior to and subsequent to heat treat-

ment are displayed in Figs. 2(a)–2(f). It can be observed from Figs. 2(a)–2(c) that the unheated membranes are smooth and flat, the PAA and PAN membranes display light yellow and white, respectively, and the PAA/PAN composite membrane exhibits a color that was comparable to PAA. After 2-h heat treatment at 300 °C (Figs. 2d–2f), the appearances of these three membranes change evidently. The PI/oPAN composite membrane appeared brown in between the yellow and black appearances of the individual PI and oPAN membranes. These color changes are inseparable from the change in chemical structure, which will be discussed later.

Figs. 2(g)–2(l) display the typical surface SEM images of these membranes. As depicted in Figs. 2(g)–2(i), the electrospun membranes without heat treatment were all composed of randomly oriented fibers, which were piled together to build a 3D porous network structure. The smooth surface of the PI nanofibrous membrane obtained after heat treatment resembled that of PAA (Fig. 2j), whereas the obtained oPAN membrane exhibited irregular bubbles and holes on its surface and no longer had a fibrous structure (Fig. 2k). This was because 300 °C exceeds PAN's glass transition temperature (104 °C) and nearly as high as PAN's melting point (317 °C), causing fibers to contact, adhere together and melt. Consequently, the PI/oPAN composite membrane obtained after the heat treatment retained the fibrous network structure of its surface because of the supporting PI nanofibers, but there were also clear adhesion spots referring to the oPAN component (Fig. 2l).

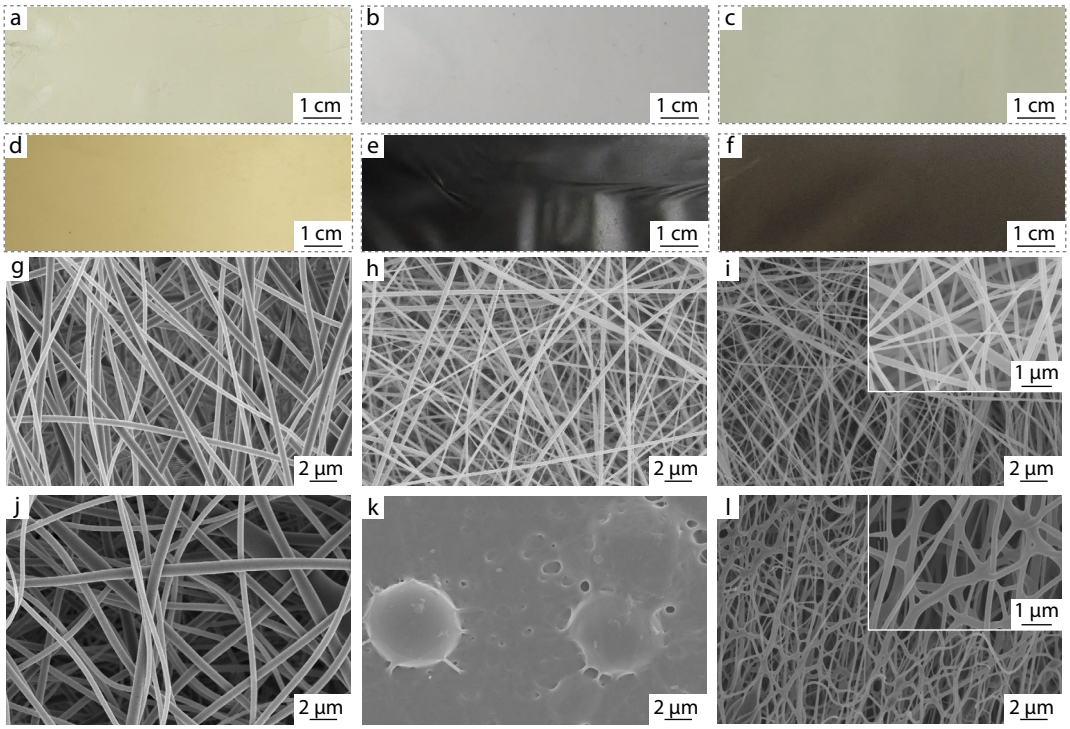

Fig. 2 (a–f) Photographs and (g–l) SEM images of nanfibrous membranes before (a–c, g–i) and after (d–f, j–l) heat treatment: (a, g) PAA, (b, h) PAN, (c, i) PAA/PAN, (d, j) PI, (e, k) oPAN, (f, l) PI/oPAN.

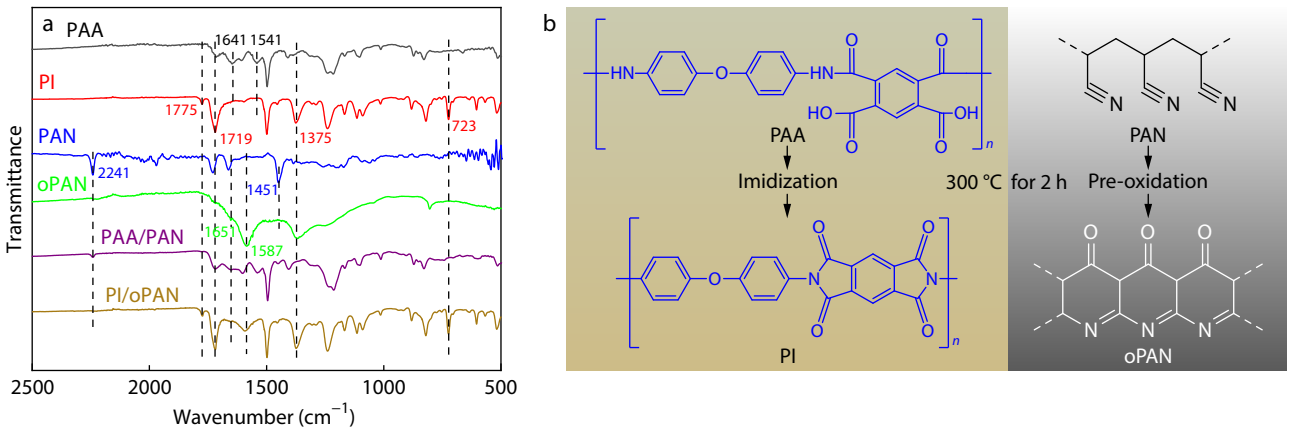

Fig. 3 (a) FTIR spectra of PAA, PI, PAN, oPAN, PAA/PAN and PI/oPAN membranes; (b) Chemical structure changes during the imidization of PAA and pre-oxidation of PAN.

https://doi.org/10.1007/s10118-024-3180-y

Chemical Structure Analysis

The main chemical structure changes of single-component and composite nanofibrous membranes experienced heat treatment were further explored after figuring out the morphological changes. Fig. 3(a) displays the FTIR spectra of PAA, PI, PAN, oPAN, PAA/PAN and PI/oPAN membranes plotted in the spectral region from 2500 cm^{-1} to 500 cm^{-1}. The C=O vibration at 1641 cm^{-1} and the C—N—H stretching vibration at 1541 cm^{-1} are the most important characteristic bands of PAA,[31] and these two bands disappear from the spectrum of PI obtained after 2 h treatment at 300 °C. Meanwhile, there are apparent bands respectively appearing at 1775 and 1719 cm^{-1}, which were caused by the asymmetric and symmetric stretching vibrations of the C=O derived from the imine ring. Other new band values at 1375 and 723 cm^{-1} are respectively on behalf of the C—N stretching vibration and C=O formation vibration.[32] These above findings were evidence that the PAA had been successfully imidized to PI after heat treatment.

PAN will be pre-oxidized upon heating under high temperature, *e.g.*, 200–300 °C, for a long period, and a series of cyclization, dehydrogenation, oxidation, cross-linking, *etc.*, reactions will accompany during the pre-oxidation process.[33] When compares the spectra of PAN and oPAN, it can be found that the absorption band of C=N at 1587 cm^{-1} has a distinct rise in intensity, while the absorption band of C≡N at 2241 cm^{-1} gradually decreases (Fig. 3a). This suggested that, during the heating process, a cyclization reaction had taken place, resulting in the C≡N being cyclized to form C=N and the PAN linear molecular chain gradually changing into a ring ladder network structure (Fig. 3b). Meanwhile, the $-CH_2$ absorption band intensity at 1451 cm^{-1} was significantly weakened, which also indicated that a dehydrogenation reaction occurred, converting the $-CH_2$ to the —CH and forming a C=C conjugate structure. However, the C=C stretching vibration absorption band created an overlapping band with the N—H and C=N stretching vibration absorption bands since they all were present at approximately 1587 cm^{-1}. Furthermore, the appearance of conjugated C=O absorption band at 1651 cm^{-1} suggested an oxidation reaction occurs.[34,35] As per the aforementioned findings, PAN has already undergone pre-oxidation to become oPAN after the heat treatment.

For the PAA/PAN and PI/oPAN composite membranes, the variations of the characteristic peaks in the spectra almost combined the changes of both components, demonstrating that PAA had been converted to PI and PAN had been pre-

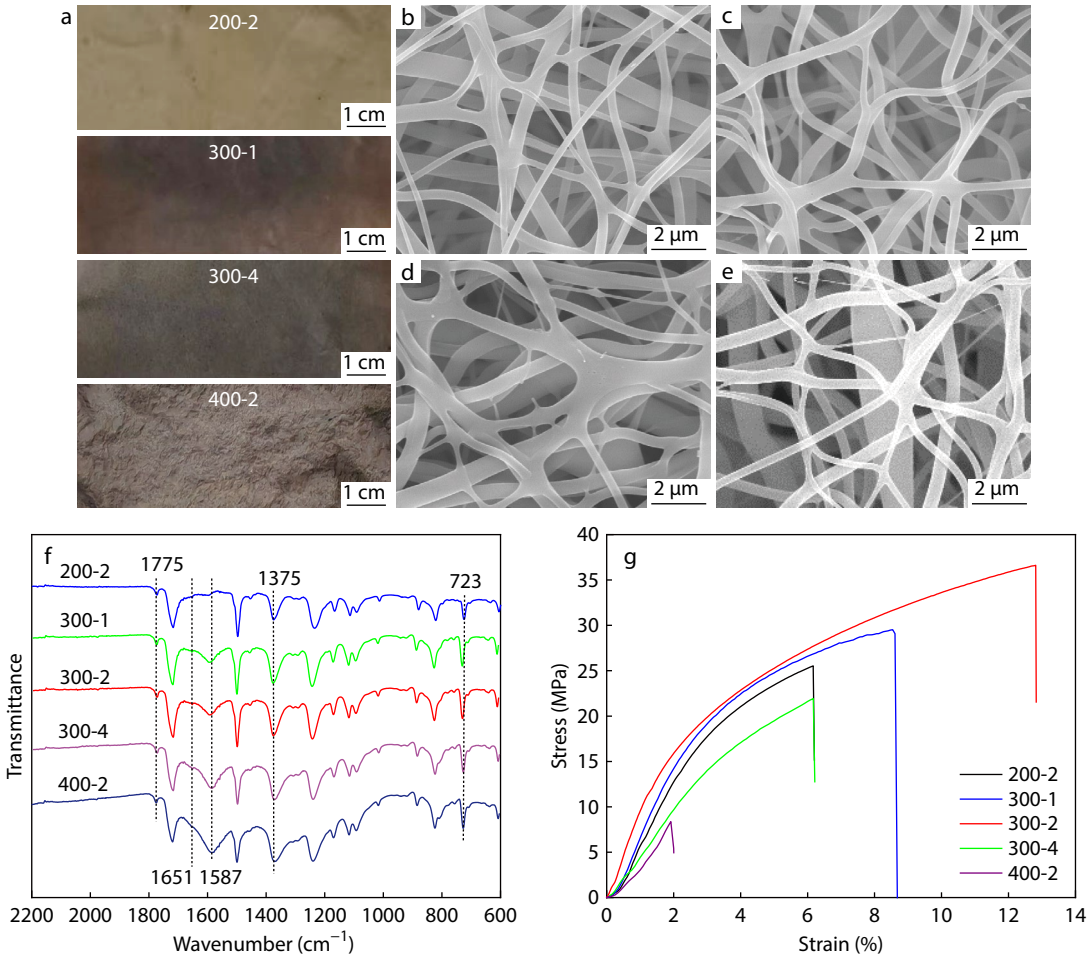

Fig. 4 (a) Photographs and (b–e) SEM images of composite membranes after heat treatment under different temperature-time conditions: (b) 200-2, (c) 300-1, (d) 300-4 and (e) 400-2; (f) FTIR spectra and (g) typical stress-stain curves of the composite membranes after heat treatment under different conditions.

https://doi.org/10.1007/s10118-024-3180-y

oxidized to oPAN in the composite membrane. Moreover, the appearance color of the membranes varies dramatically throughout the heating process due to the production of these groups including C=C, C=O, and C=N.

Effects of Heat Treatment Conditions

We are aware of the impact of heat treating a material to 300 °C for 2 h based on the analysis above. Indeed, we have also investigated how various heat treatment conditions affect the composite membranes' morphologies, structure, and properties (Fig. 4). The membrane, heat treated at a temperature of *x* for hours of *y*, was recorded as *x*-*y*. It was found that the color under different heat treatment conditions was clearly distinct (Fig. 4a), and the adhesion degree between fibers in these membranes was also slightly different (Figs. 4b–4e), which was closely related to the change of their chemical structure. As presented in Fig. 4(f), the typical bands of PI (at 1775, 1375 and 723 cm^{-1}) were clearly visible after 2 h of treatment at 200 °C, whereas the oPAN's feature bands (at 1651 and 1587 cm^{-1}) were not. Both in the composite membrane (300-1) were noticeable when subjected to 300 °C for 1 h. The characteristic peaks of PI did not change significantly when the temperature or time of the heat treatment increased, but the characteristic peak intensity of oPAN did, suggesting that increasing the temperature and time would increase the degree of pre-oxidation of PAN. These structural variations played significant roles in the mechanical properties of the composite membranes (Fig. 4g). When the temperature was not greater than 300 °C and the duration was not more than 2 h, the tensile strength and elongation at break progressively improved as the temperature or time increased. While the strength and elongation of 300-4 membrane were drastically decreased possibly due to the deterioration and degradation of fibers at high temperature for long time. In particular, the 400-2 sample had become extremely brittle, easy to break and then presented a very poor mechanical property. Therefore, taking the chemical structure and property into account, the heat treatment condition of 300 °C for 2 h was selected for the following PI/oPAN composite separator fabrication and performance measurements.

Porosity and Wettability

Fig. 5(a) displays different separators' porosities. It was worth noting that the porosities of PI and PAN membranes were greater than PP (40.8%), at 74.4% and 80.5%, respectively. This could be attributed to the nanofibrous membrane's 3D porous network structure generated by electrospinning technique. The PI/oPAN separator's porosity was 71.7%, lower than that of PI and PAN, which was because a number of adhesion points between fibers can be found in the composite separator due to the pre-oxidation of PAN. It should be pointed out that the PAN rather than oPAN is selected for the following performance comparison, because the mechanical properties of the pure oPAN membrane treated at 300 °C for 2 h were so poor that it is easily broke upon touch, and thus it is inappropriate for the porosity, wettability, thermal, mechanical and electrochemical properties tests.

The separator's electrolyte wettability has an appreciable impact on the assembled batteries' electrochemical performance.[36] The changes over time of electrolyte contact angles of different separators were presented in Fig. 5(b). As seen, the PP separator exhibited the highest contact angle and its electrolyte did not spread out after 100 s. The PI and

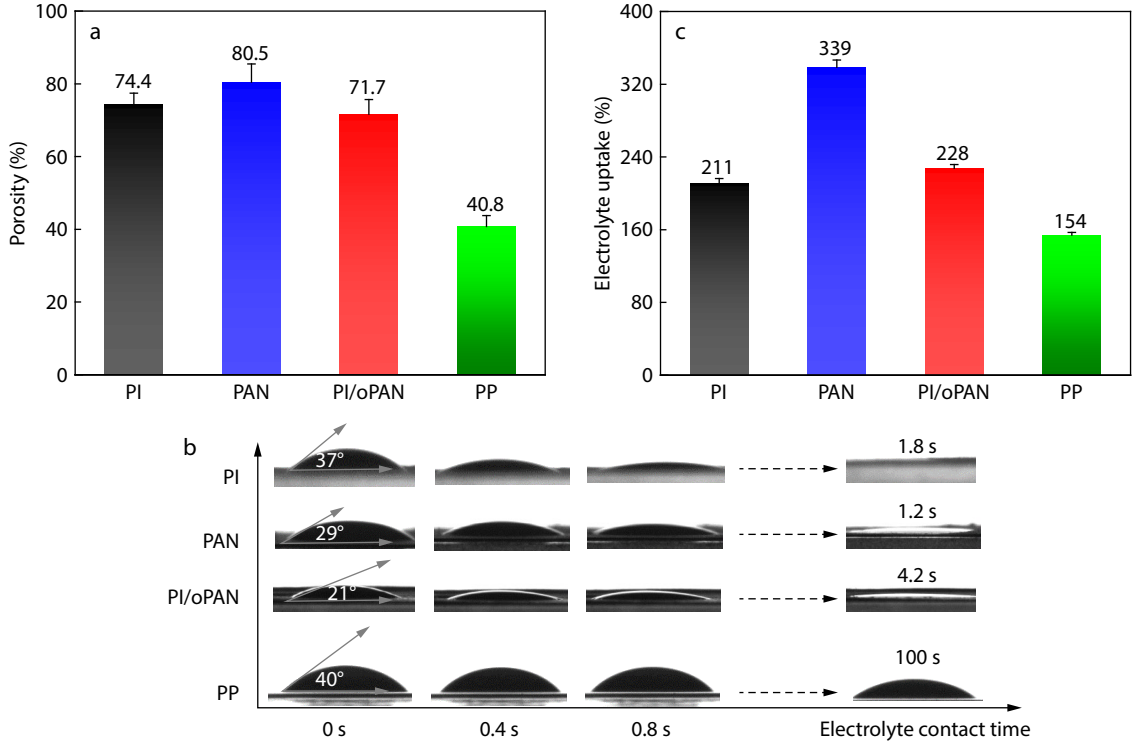

Fig. 5 (a) The porosity, (b) the electrolyte contact angle changing over time and (c) the electrolyte uptake of diverse separators (PI, PAN, PI/oPAN and commercial PP).

PAN separators' electrolyte contact angles were 37° and 29°, respectively, and their complete spreading times were very short, only 1.8 and 1.2 s. This could be explained by the electrospun separators' good pore structure, which allows electrolytes to diffuse rapidly, together with the fact that the imide groups of PI and the C═N of oPAN improved the separators' electrolyte affinity. The wetting time of the PI/oPAN composite separator was 4.2 s longer than that of the single component, while having the least contact angle of 21°. The full spreading time increase could be ascribed to the pre-oxidation partially destroying the PAN fiber morphology and limiting the electrolyte diffusion on oPAN. The contact angle decreased as a result of the adhesion between oPAN and PI fibers changing the pore size distribution.

Moreover, the electrolyte uptake behavior was illustrated in Fig. 5(c). The electrospun separators all had greatly elevated electrolyte uptake values of over 200%, when compared with the PP separator (154%), which was because their 3D porous structure could absorb a huge quantity of electrolyte. It can be found that the electrolyte uptake value of PI/oPAN separator was lower than that of PAN, which could be attributed to the reduced porosity and the reduced polarity caused by the changed chemical structure of PAN after pre-oxidation.

Thermal and Mechanical Properties

Different separators' thermal and mechanical properties were investigated and presented in Fig. 6. The composite PI/oPAN separators exhibited nearly the same thermal stability as PI (Fig. 6a), starting to decompose at a temperature of around 500 °C and losing roughly 20% of its weight at 600 °C. While the PAN separator began to lose weight from 300 °C, and it lost approximately 62% of its weight at 600 °C. Fig. 6(b) displays the optical images of various separators that were heat-treated at different temperatures. Benefiting from PI and oPAN, the PI/oPAN composite separator demonstrated good thermal dimensional stability, which could maintain dimensional integrity within 200 °C. In contrast to commercial PP, which experienced significant shrinkage at 150 °C, and PAN, which curled at the same temperature due to its nonuniform thermal shrinkage, the PI/oPAN separator proved advantageous for LIBs' safe use in environments with high temperatures.

Figs. 6(c) and 6(d) show the tensile and puncture properties of single-component and composite separators. Here, the commercial PP separator is not selected for comparison due to its dry unidirectional stretching manufacture process that is totally different from the electrospinning. As compared to the pure PI membrane which had a tensile strength of 12.5 MPa with elongation at break of 5.1%, and puncture load of 1.17 N, the PI/oPAN separator had nearly 3 times enhancement of which the tensile strength reached up to 36.6 MPa, elongation at break improved to 12.8%, and puncture load up to 3.58 N. Such great improvement in mechanical performance could be attributed to the adhesion phenomenon re-

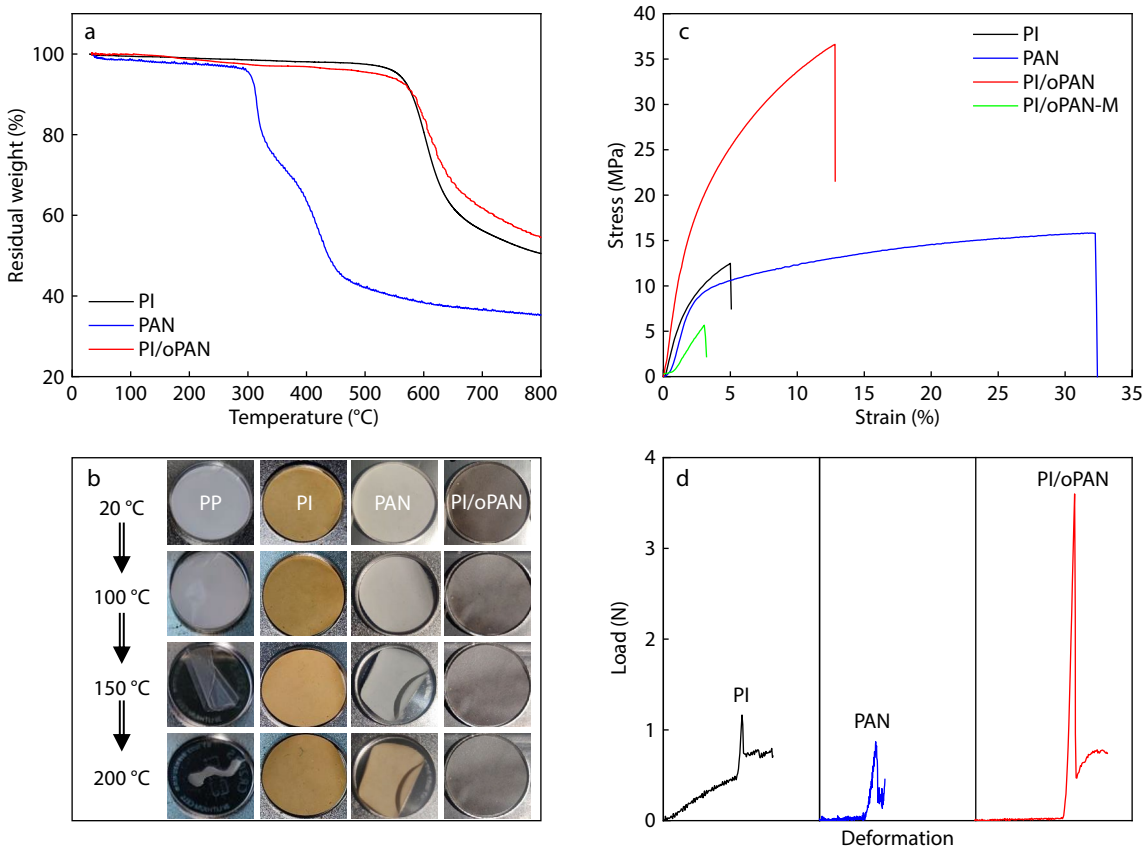

Fig. 6 (a) Thermogravimetric (TG) thermegrams, (b) photographs under a series of temperatures (room temperature, 100, 150 and 200 °C) for 30 min, (c) stress-strain curves and (d) puncture load-deformation curves of single-component and composite separators (PI/oPAN-M was fabricated by hybrid solution electrospinning rather than the cross-electrospinning).

https://doi.org/10.1007/s10118-024-3180-y

sulting from the pre-oxidation of the PAN fibers at 300 °C. The decrease in the elongation of the PI/oPAN separator, compared to the high elongation (32.2%) of the PAN separator, was created by the ladder structure generated during the PAN pre-oxidation process, which weakened the slip and stretching ability between molecules.[30]

Meanwhile, the tensile properties of the PI/oPAN-M membrane prepared by solution hybrid electrospinning were tested for comparison. The solution hybrid electrospinning is a frequently used method which means mixing PAA and PAN solutions together and then electrospinning it to get the PI/oPAN-M, while the PI/oPAN is produced by simultaneously electrospinning the separate solutions using two sets of spinning equipment. Results showed that the PI/oPAN-M's tensile strength and elongation at break were only 5.1 MPa and 4.1%, respectively, quite lower than those of PI/oPAN created by the cross-electrospinning technique. Therefore, it can be concluded that the cross-electrospinning method did significantly improve the composite membrane's mechanical properties.

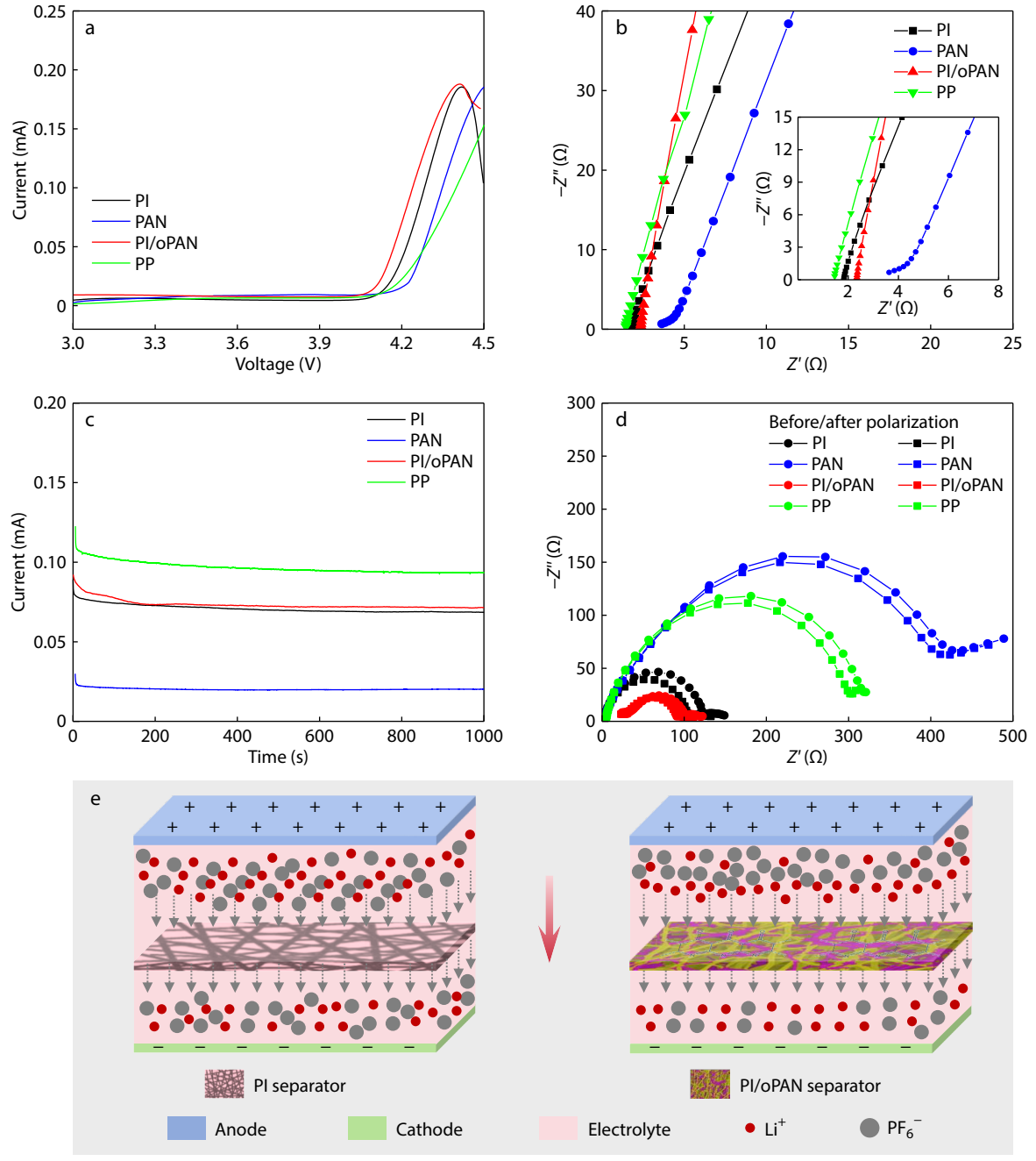

Fig. 7 (a) LSV curves of stainless steel/separator/Li coin cells; (b) Nyquist plots of stainless steel/separator/stainless steel coin cells; (c) Chronoamperometry profiles and (d) the related EIS analyses (before and after polarization) of Li/separator/Li coin cells with PI, PAN, PI/oPAN and PP separators; (e) Schematic illustration of the transport capacity of Li^+ between PI and PI/oPAN separators.

https://doi.org/10.1007/s10118-024-3180-y

Electrochemical Properties

The separator's electrochemical stability during the voltage range of battery system's operating is of great importance in practical applications.[37] The voltammetry curves of PI, PAN, PI/oPAN and PP separators were presented in Fig. 7(a). When a sharp increase occurs in current, it marks the onset of the decomposition of the electrolyte, which decides the limitation of electrochemical oxidation.[38,39] As shown, the PI/oPAN composite separator presented an anodic stability value up to 4.11 V, which was similar to that of PI, PAN and PP. This result indicated that they all had favorable interfacial compatibility and could ensure the stable operation of LIBs in practical applications.

The ion transport capacity of separators was explored, since one of the separator's main functions is to provide access for Li^+ transport. Fig. 7(b) shows the Nyquist plots of the stainless steel/separator/stainless steel coin cells. The bulk resistance was determined from these plots, and then the ionic conductivity value was calculated. The bulk resistances of PI, PAN, PI/oPAN and PP separators were 1.73, 4.19, 2.28 and 1.39 Ω, respectively, and the related ionic conductivities were respectively 1.20, 0.69, 0.88 and 0.63 $mS·cm^{-1}$. The lithium-ion transference number (t_{Li^+}) is another key indicator of a separator's Li^+ transport ability besides ionic conductivity, which reflects the effective electrochemical processes resulting from Li^+ transport. A low t_{Li^+} is more likely to trigger severe concentration polarization, lead to discharge capacity loss and associated negative consequences.[40] The chronoamperometry profiles and corresponding EIS analyses of Li/separator/Li coin cells with PI, PAN, PI/oPAN and PP separators were presented in Figs. 7(c) and 7(d), which provided the t_{Li^+} values. The t_{Li^+} values of PI, PAN, PI/oPAN and PP were 0.45, 0.52, 0.60 and 0.29, respectively. The separator's ion transport capacity, as reflected by values of ionic conductivity and t_{Li^+}, is illustrated in Fig. 7(e). The pre-oxidation of PAN reduced its porosity and electrolyte uptake, so its number of ions *via* PI/oPAN separator was less than that *via* the PI separator. Meanwhile, the conjugated systems of the C=N generated in the oPAN component and the polar groups in the oPAN conjugated system had high affinity with the cations and thus could promote Li^+ transporting through the separator, resulting in a large amount of Li^+ transported by the PI/oPAN separator and highly effective electrochemical processes.

Battery Performance

In order to prove the prepared separators' application in LIBs, $Li/LiFePO_4$ coin cells assembled with single-component and composite separators were operated at a rate of 1 C, with the PP separator also tested for comparison. The relationships of the coin cell's discharge capacity and coulombic efficiency with cycle number are displayed in Fig. 8(a). It could be noticed that the discharge capacity decreased and the coulomb efficiency remained almost constant at above 98.3% with increasing number of cycles. In particular, the coin cell using the PI/oPAN separator had an initial discharge capacity up to 138 $mAh·g^{-1}$ and a capacity retention ratio of 91.0% after 100 cycles, well above that of cells with PI (129 $mAh·g^{-1}$, 96.6%), PAN (110 $mAh·g^{-1}$, 87.8%) and commercial PP (110 $mAh·g^{-1}$, 85.2%).

The rate capabilities of these assembled coin cells underlain PI, PAN, PI/oPAN and PP separators were studied by operating several current densities 0.2, 0.5, 1, 2 and 5 C and then down to 0.2 C, respectively, for 5 cycles. From Fig. 8(b), it was shown that the cells' discharge capacity gradually decreased as the rate increased. At 0.2 C, the cell that used the PP separator had the lowest discharge capacity of about 129 $mAh·g^{-1}$, and then reduced to 23 $mAh·g^{-1}$ at 5 C. By contrast, the cell using the PI/oPAN separator showed a greater discharge capacity up to 137 $mAh·g^{-1}$ at 0.2 C, decreasing to 57 $mAh·g^{-1}$ at 5 C. On the other hand, the discharge capacities of cells with PI, PAN and PI/oPAN separators were quite near the original capacities as the rate returned to 0.2 C, while the capacity of cell using the PP separator was diminished by about 16.3%. This good battery performance could be explained by the PI/oPAN separator's good electrolyte wettability and Li^+ migration capability.

Table 1 lists the materials, preparation methods, and separators' properties of other work, including work on the composite of PAN and PI, and some recent reports on PI or PAN. The comparison revealed that the PI/oPAN separator prepared in this work by cross-electrospinning combined with heat treatment process had the highest tensile strength and acceptable other comprehensive properties, thus presenting great potentials as the separator for lithium batteries with high performance.

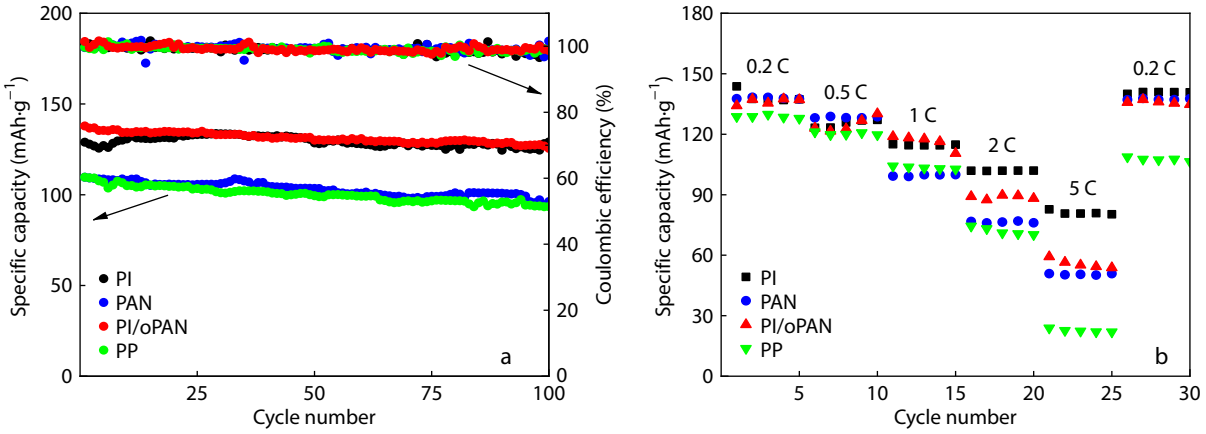

Fig. 8 (a) Cycling performance and corresponding coulombic efficiency and (b) rate capabilities of the coin cells ($LiFePO_4$ cathode, Li anode) with PI, PAN, PI/oPAN and PP separators.

https://doi.org/10.1007/s10118-024-3180-y

Table 1 Performance comparisons between PI or PAN composite separators with PI/oPAN separators.

Materials	Processing method	Thickness (μm)	Porosity (%)	Electrolyte uptake (%)	Dimensionally stability temperature (°C)	Tensile strength (Mpa)	Ionic conductivity ($mS·cm^{-1}$)	Cycling performance (capacity retention)	Battery (cathode/ anode)	Reference
PAN/PI	Blend electrospinning	30	87	487	200	7.01±0.82	18.77×10^{-4}	/	$LiFePO_4$/Li	[24]
PAN/ODA/ PMDA	Blend electrospinning	25–30	73.36	558.63	250	32.5	2.39	95.57% after 100 cycles at 0.5 C	$LiCoO_2$/ graphite	[25]
SiO_2/ PAN/PI	Blend electrospinning	30	70	491	160	18.9	2.7	93% after 200 cycles at 1 C	$LiCoO_2$/ graphite	[26]
PI/PAN/PI	Electrospinning, non-solvent phase separation and pressed lamination	75	88.7	554.2	200	18.12	0.69	94.3 % after 100 cycles at 1 C	$LiFePO_4$/Li	[31]
PI/PS	Blend electrospinning	24	81	540.2	250	26.4	1.1	80% at 10 C after 1600 cycles	$LiFePO_4$/Li	[41]
PI/DBDPE/ CNF	Phase inversion	18	81	192	200	25.4	0.45	/	$LiFePO_4$/Li	[42]
PAN/PVDF	Coaxial electrospinning	60	81.61	804.3	170	3.6	1.62	90.7% at 5 C after 125 cycles	$LiCoO_2$/Li	[12]
PAN/PVDF-HFP/PVP	Blend electrospinning	38	70.7	584.2	200	20.05	1.78	95.4% at 0.5 C after 50 cycles	$LiCoO_2$/ graphite	[43]
PAN@PVDF -HFP/BM	Coaxial electrospinning	120–150	85.2	872.8	130	5.8	3.98	93.3% at 0.2 C after 200 cycles	$LiFePO_4$/Li	[44]
PI/oPAN	Cross-electrospinning	45	71.7	228	200	**36.6**	0.88	91.0% at 1C after 100 cycles	$LiFePO_4$/Li	This work

CONCLUSIONS

In summary, a new strategy for the preparation of PI/oPAN separator by cross-electrospinning combined with heat treatment process was proposed, and the impacts of heat treatment conditions were investigated upon the morphologies, structure, and properties of the composite membranes, and an optimal treatment process (300 °C for 2 h) was selected. Thanks to PI and pre-oxidation of PAN, the composite membrane maintained dimensional stability at 200 °C, and the tensile and puncture properties were about 3 times of neat PI. The adhesive structure generated during the pre-oxidation of PAN optimized the pore size and distribution, while the polar groups in the oPAN conjugated system interacted with Li^+, thus improving the Li^+ migration capability of the composite separator and making the cycling and rate performance of the cell more excellent than cells with PI or PAN nanofibrous separator. Therefore, this research offered an advanced approach for accelerating the creation of LIBs separators with desirable electrochemical performance and robust mechanical strength.

Conflict of Interests

The authors declare no interest conflict.

Data Availability Statement

The related data of this paper are data that should not be shared, and can be obtained from the author for reasonable reasons. The author's contact information: zzwei@suda.edu.cn.

ACKNOWLEDGMENTS

This work was financially supported by the Natural Science Foundation of the Jiangsu Higher Education Institutions of China (No. 22KJA480004) and the Key Laboratory of Flame Retardancy Finishing of Textile Materials, CNTAC (No. Q811580421).

REFERENCES

1 Sasaki, T.; Ukyo, Y.; Novak, P. Memory effect in a lithium-ion battery. *Nat. Mater.* **2013**, *12*, 569–575.
2 Notter, D. A.; Gauch, M.; Widmer, R.; Wäger, P.; Stamp, A.; Zah, R.; Althaus, H. J. Contribution of Li-ion batteries to the environmental impact of electric vehicles. *Environ. Sci. Technol.* **2010**, *44*, 6550–6556.
3 Zeng, X. Q.; Li, M.; Abd El-Hady, D.; Alshitari, W.; Al-Bogami, A. S.; Lu, J.; Amine, K. Commercialization of lithium battery technologies for electric vehicles. *Adv. Energy Mater.* **2019**, *9*, 1900161.
4 Jang, J.; Oh, J.; Jeong, H.; Kang, W.; Jo, C. A review of functional separators for lithium metal battery applications. *Materials* **2020**, *13*, 4625.
5 Yang, Y.; Chen, Z.; Lv, T.; Dong, K.; Liu, Y.; Qi, Y.; Cao, S.; Chen, T. Ultrafast self-assembly of supramolecular hydrogels toward novel flame-retardant separator for safe lithium ion battery. *J. Colloid Interface Sci.* **2023**, *649*, 591–600.
6 Francis, C. F. J.; Kyratzis, I. L.; Best, A. S. Lithium-ion battery separators for ionic-liquid electrolytes: a review. *Adv. Mater.* **2020**, *32*, 1904205.
7 Yu, J.; Dong, N.; Liu, B.; Tian, G.; Qi, S.; Wu, D. A newly-developed heat-resistance polyimide microsphere coating to enhance the

thermal stability of commercial polyolefin separators for advanced lithium-ion battery. *Chem. Eng. J.* **2022**, *442*, 136314.
8 Lee, H.; Yanilmaz, M.; Toprakci, O.; Fu, K.; Zhang, X. W. A review of recent developments in membrane separators for rechargeable lithium-ion batteries. *Energy Environ. Sci.* **2014**, *7*, 3857–3886.
9 Ding, L.; Zhang, C.; Wu, T.; Yang, F.; Lan, F.; Cao, Y.; Xiang, M. Effect of temperature on compression behavior of polypropylene separator used for Lithium-ion battery. *J. Power Sources* **2020**, *466*, 228300.
10 Yu, Y.; Liu, M.; Chen, Z. Y.; Zhang, Z. H.; Qiu, T.; Hu, Z. X.; Xiang, H. X.; Zhu, L. P.; Xu, G. Y.; Zhu, M. F. Advances in Nonwoven-based separators for lithium-ion batteries. *Adv. Fiber Mater.* **2023**, *5*, 1827–1851.
11 Wang, L.; Liu, F.; Shao, W.; Cui, S.; Zhao, Y.; Zhou, Y.; He, J. Graphite oxide dopping polyimide nanofiber membrane via electrospinning for high performance lithium-ion batteries. *Compos. Commun.* **2019**, *16*, 150–157.
12 Gao, X.; Sheng, L.; Yang, L.; Xie, X.; Li, D.; Gong, Y.; Cao, M.; Bai, Y.; Dong, H.; Liu, G.; Wang, T.; Huang, X.; He, J. High-stability core-shell structured PAN/PVDF nanofiber separator with excellent lithium-ion transport property for lithium-based battery. *J. Colloid Interface Sci.* **2023**, *636*, 317–327.
13 Miao, Y. E.; Zhu, G. N.; Hou, H. Q.; Xia, Y. Y.; Liu, T. X. Electrospun polyimide nanofiber-based nonwoven separators for lithium-ion batteries. *J. Power Sources* **2013**, *226*, 82–86.
14 Shayapat, J.; Chung, O. H.; Park, J. S. Electrospun polyimide-composite separator for lithium-ion batteries. *Electrochim. Acta* **2015**, *170*, 110–121.
15 Lee, J. H.; Manuel, J.; Choi, H.; Park, W. H.; Ahn, J. H. Partially oxidized polyacrylonitrile nanofibrous membrane as a thermally stable separator for lithium ion batteries. *Polymer* **2015**, *68*, 335–343.
16 Woo, J. C.; Youk, J. H.; Kim, D. S.; Ahn, J. H. Heating effect on physical and electrochemical properties of nanofibrous polyacrylonitrile separator for lithium batteries. *J. Nanosci. Nanotechnol.* **2014**, *14*, 9232–9236.
17 Hwang, K.; Kwon, B.; Byun, H. Preparation of PVdF nanofiber membranes by electrospinning and their use as secondary battery separators. *J. Membrane Sci.* **2011**, *378*, 111–116.
18 Bicy, K.; Gueye, A. B.; Rouxel, D.; Kalarikkal, N.; Thomas, S. Lithium-ion battery separators based on electrospun PVDF: a review. *Surf. Interfaces* **2022**, *31*, 101977.
19 Yanilmaz, M. Evaluation of electrospun PVA/SiO_2 nanofiber separator membranes for lithium-ion batteries. *J. Text. I.* **2020**, *111*, 447–452.
20 Hao, J. L.; Lei, G. T.; Li, Z. H.; Wu, L. J.; Xiao, Q. Z.; Wang, L. A novel polyethylene terephthalate nonwoven separator based on electrospinning technique for lithium ion battery. *J. Membrane Sci.* **2013**, *428*, 11–16.
21 Yu, H.; Shi, Y.; Yuan, B.; He, Y.; Qiao, L.; Wang, J.; Lin, Q.; Chen, Z.; Han, E. Recent developments of polyimide materials for lithium-ion battery separators. *Ionics* **2021**, *27*, 907–923.
22 Ding, Y.; Hou, H.; Zhao, Y.; Zhu, Z.; Fong, H. Electrospun polyimide nanofibers and their applications. *Prog. Polym. Sci.* **2016**, *61*, 67–103.
23 Lu, Z. H.; Sui, F.; Miao, Y. E.; Liu, G. H.; Li, C.; Dong, W.; Cui, J.; Liu, T. X.; Wu, J. X.; Yang, C. L. Polyimide separators for rechargeable batteries. *J. Energy Chem.* **2021**, *58*, 170–197.
24 Li, L.; Liu, P.; Fu, Q. S.; Gong, Y.; Zhang, S. R.; He, H. J.; Chen, J. Study on preparation of polyacrylonitrile/polyimide composite lithium-ion battery separator by electrospinning. *J. Mater. Res.* **2019**, *34*, 642–651.
25 Ul Arifeen, W.; Kim, M.; Ting, D.; Kurniawan, R.; Choi, J.; Yoo, K.; Ko, T. J. Hybrid thermal resistant electrospun polymer membrane as the separator of lithium ion batteries. *Mater. Chem. Phys.* **2020**, *245*, 122780.
26 Arifeen, W. U.; Choi, J.; Yoo, K.; Shim, J.; Ko, T. J. A nano-silica/polyacrylonitrile/polyimide composite separator for advanced fast charging lithium-ion batteries. *Chem. Eng. J.* **2021**, *417*, 128075.
27 Chen, S. L.; Han, D. H.; Hou, H. Q. High strength electrospun fibers. *Polym. Adv. Technol.* **2011**, *22*, 295–303.
28 Rahaman, M. S. A.; Ismail, A. F.; Mustafa, A. A review of heat treatment on polyacrylonitrile fiber. *Polym. Degrad. Stabil.* **2007**, *92*, 1421–1432.
29 Qin, X.-H. Structure and property of electrospinning PAN nanofibers by different preoxidation temperature. *J. Therm. Anal. Calorim.* **2010**, *99*, 571–575.
30 Zou, Y.; Jiang, S.; Hu, X.; Xu, W.; Chen, Z.; Liu, K.; Hou, H. Influence of pre-oxidation on mechanical properties of single electrospun polyacrylonitrile nanofiber. *Mater. Today Commun.* **2021**, *26*, 102069.
31 Cao, D.; Deng, J.; Jiang, L.; Li, X.; Zhang, G. Designing polyimide/polyacrylonitrile/polyimide sandwich composite separator for rechargeable lithium-ion batteries. *J. Energy Storage* **2022**, *55*, 105496.
32 Li, M. L.; Sheng, L.; Zhang, H.; Yang, Y.; Xu, R.; Bai, Y. Z.; Song, S. J.; Liu, G. J.; Wang, T.; Huang, X. L.; He, J. P. Effect of the heat treatment temperature on mechanical and electrochemical properties of polyimide separator for lithium ion batteries. *J. Mater. Sci.* **2020**, *55*, 16158–16170.
33 Morita, K.; Murata, Y.; Ishitani, A.; Murayama, K.; Ono, T.; Nakajima, A. Characterization of commercially available PAN (Polyacrylonitrile)-based carbon-fibers. *Pure Appl. Chem.* **1986**, *58*, 455–468.
34 Liu, Y.; Liu, Y.; Shang, L.; Ao, Y. H. Study on the structural evolution of polyacrylonitrile fibers in stepwise heat treatment process and its relationship with properties. *J. Appl. Polym. Sci.* **2022**, *139*, e52077.
35 Huang, H.; Yu, B.; Wang, X. A high thermal stable pre-oxidized polyacrylonitrile nanofiber separator for lithium-ion battery. *J. Appl. Polym. Sci.* **2023**, *140*, e54410.
36 Liu, J. H.; Wang, P.; Gao, Z.; Li, X.; Cui, W.; Li, R.; Ramakrishna, S.; Zhang, J.; Long, Y. Z. Review on electrospinning anode and separators for lithium ion batteries. *Renew. Sust. Energ. Rev.* **2024**, *189*, 113939.
37 Zhai, Y. Y.; Wang, N.; Mao, X.; Si, Y.; Yu, J. Y.; Al-Deyab, S. S.; El-Newehy, M.; Ding, B. Sandwich-structured PVdF/PMIA/PVdF nanofibrous separators with robust mechanical strength and thermal stability for lithium ion batteries. *J. Mater. Chem. A* **2014**, *2*, 14511–14518.
38 Zhang, H.; Zhang, Y.; Yao, Z. K.; John, A. E.; Li, Y.; Li, W. S.; Zhu, B. K. Novel configuration of polyimide matrix-enhanced cross-linked gel separator for high performance lithium ion batteries. *Electrochim. Acta* **2016**, *204*, 176–182.
39 Xing, J.; Fan, W.; Li, J.; Wang, Z.; Wei, Z.; Zhao, Y. Orientation gradient architecture of nanofibrous separator towards mechanical enhancement and ion transport acceleration for lithium-ion batteries. *Electrochim. Acta* **2023**, *441*, 141794.
40 Pozyczka, K.; Marzantowicz, M.; Dygas, J. R.; Krok, F. Ionic conductivity and lithium transference number of poly(ethylene oxide): LiTFSI system. *Electrochim. Acta* **2017**, *227*, 127–135.

https://doi.org/10.1007/s10118-024-3180-y

41 Wang, Y.; Guo, M.; Fu, H.; Wu, Z.; Zhang, Y.; Chao, G.; Chen, S.; Zhang, L.; Liu, T. Thermotolerant separator of cross-linked polyimide fibers with narrowed pore size for lithium-ion batteries. *J. Membr. Sci.* **2022**, *662*, 121004.
42 Liu, Y.; Li, C.; Li, C. X.; Xu, L. H.; Zhou, S.; Zhang, Z.; Zhang, J. X.; Soham, D.; Fan, R.; Liu, H.; Chen, G.; Li, Y. Y.; Ling, T.; Li, Z. P.; Tao, J. S.; Wan, J. Y. Porous, robust, thermally stable, and flame retardant nanocellulose/polyimide separators for safe lithium-ion batteries. *J. Mater. Chem. A* **2023**, *11*, 23360–23369.
43 Leng, X.; Yang, M.; Li, C.; Arifeen, W. U.; Ko, T. J. High-performance separator for lithium-ion battery based on dual-hybridizing of materials and processes. *Chem. Eng. J.* **2022**, *433*, 133773.
44 Chen, Z.; Guan, M. D.; Cheng, Y. W.; Li, H.; Ji, G. J.; Chen, H.; Fu, X. G.; Awuye, D. E.; Zhu, Y. B.; Yin, X. C.; Man, Z. M.; Wu, C. Boehmite-enhanced poly(vinylidene fluoride-*co*-hexafluoropropylene)/polyacrylonitrile (PVDF-HFP/PAN) coaxial electrospun nanofiber hybrid membrane: a superior separator for lithium-ion batteries. *Adv. Compos. Hybrid Mater.* **2023**, *6*, 219.

https://doi.org/10.1007/s10118-024-3180-y